

# The effect of $\text{TiO}_2$ on the microstructural and electrical properties of low voltage varistor based on $(\text{Sn},\text{Ti})\text{O}_2$ ceramics

D. R. Leite, M. Cilense, M. O. Orlandi\*, P. R. Bueno, E. Longo, and J. A. Varela

Institute of Chemistry, São Paulo State University, UNESP, Araraquara, SP, Brazil

Received 9 June 2007, revised 17 September 2009, accepted 21 September 2009

Published online 30 October 2009

PACS 61.72.Dd, 61.72.Ff, 84.32.Ff, 84.37.+q

\* Corresponding author: e-mail orlandi@iq.unesp.br, Phone: +55 16 3301 6644, Fax: +55 16 3322 0015

$\text{SnO}_2\text{-CoO-Nb}_2\text{O}_5$  ceramics doped with  $\text{TiO}_2$  have been prepared by a conventional oxide method which focuses its application on low voltage varistors. The dopant was added in 0.5 and 1.0% molar concentrations, and the samples were investigated by X-ray diffraction, scanning electron microscopy, current vs. voltage, and impedance measurements. The electron microscopy results showed an increase in the mean grain size of ceramics with the addition of  $\text{TiO}_2$ , which is related to the effect of the dopant on the matrix. The electrical

characterization showed that the addition of  $\text{TiO}_2$  in 1 mol% provides a system with a good nonlinear coefficient (8.7) and a breakdown electrical field of 617 V/cm. These results indicate that this composition can be applied as a low voltage varistor. The impedance data showed that the voltage barrier at the grain boundary is a back-to-back Schottky-type, and it was demonstrated that the addition of  $\text{TiO}_2$  does not significantly modify the barrier.

© 2010 WILEY-VCH Verlag GmbH & Co. KGaA, Weinheim

**1 Introduction** The study of advanced ceramics has increased significantly in recent years, mainly due to the necessity to understand fully the solid state phenomena (synthesis, sintering, interface properties, and the effect of additives in the intrinsic properties of material) which are mainly responsible for technological applications.  $\text{SnO}_2$  is a wide-band gap semiconductor, and the specific and unique properties presented by this material makes it very useful in many applications such as gas sensors, electrochromic devices, crystal displays, photo-detectors, solar cells, and protective coatings [1–3]. However, the predominance of non-densifying mechanisms for mass transport such as evaporation–condensation and/or surface diffusion [4] results in low densification during sintering and limits the use of  $\text{SnO}_2$  ceramics. Conversely,  $\text{SnO}_2$  dense ceramics can be obtained by the introduction of densifying agents such as  $\text{MnO}_2$  [5, 6] and  $\text{CoO}$  [7] which promote the densification of  $\text{SnO}_2$  almost to the theoretical value, focusing on its application in devices that require good electrical and mechanical properties (e.g., varistors). This behavior has been attributed to the effect of cobalt and manganese in the  $\text{SnO}_2$  lattice, leading to the formation of oxygen vacancies which promotes an increase in the diffusion coefficient of the

ions and consequently results in the densification of the  $\text{SnO}_2$  [4].

The decrease in  $\text{SnO}_2$  lattice resistivity is assigned to the presence of dopants such as  $\text{Nb}_2\text{O}_5$  [7, 8],  $\text{Sb}_2\text{O}_3$  [9], and  $\text{Ta}_2\text{O}_5$  [10]. According to Pianaro et al. [7, 8], the dopant  $\text{Nb}^{5+}$  has an ionic radius similar to  $\text{Sn}^{4+}$  acting as a donor when doping the  $\text{SnO}_2$  lattice, leading to an increase in the electron concentration.

Unlike  $\text{SnO}_2$ ,  $\text{TiO}_2$  does not need any additive for densification. Besides, it displays similar properties to those properties found in  $\text{SnO}_2$ , including its applications as a varistor [11], humidity and gas sensors [12], optic devices [13], solar cells, and as catalysts [14]. Studies have shown that dopants such as  $\text{Nb}_2\text{O}_5$  [15] and  $\text{Cr}_2\text{O}_3$  [16] act similarly in  $\text{TiO}_2$  and in  $\text{SnO}_2$ , increasing the electrical conductivity within the grains and the electrical resistivity at the grain boundary region, respectively.

The good stability of the  $\text{SnO}_2$  sensor for reducing gases combined with the good chemical stability of  $\text{TiO}_2$  at low temperatures is a strong motivation for investigating  $\text{SnO}_2\text{-TiO}_2$  solid solutions for ceramic sensor applications [17]. However, earlier studies have shown evidences that a binary system such as  $\text{SnO}_2\text{-TiO}_2$  can also display a varistor-like

behavior. Electrical and gas sensor properties (as well as the sinterability of some semiconducting oxides) are controlled by the use of dopants. A (Sn,Ti)O<sub>2</sub>-based varistor has already been achieved [18] and present low voltage varistor characteristics ( $\alpha = 9$  and  $E_b = 420$  V/cm) when the binary system is doped with 0.05 mol% of Nb<sub>2</sub>O<sub>5</sub>; the properties of varistor are highly dependent upon potential barriers in the grain boundary region.

The presence of a back-to-back Schottky-type barrier at the grain boundary region is inferred from the voltage dependence of the capacitance using the approach of Mukae et al. [19], as

$$\left(\frac{1}{C} - \frac{1}{2C_0}\right)^2 = \frac{2}{qk\epsilon_0 N_d}(\phi + V), \quad (1)$$

where  $q$  is the elementary charge,  $k$  is the dielectric constant of the material,  $\epsilon_0$  is the permittivity of free space,  $N_d$  is the donor concentration,  $\phi$  is the barrier height in the grain boundary region, and  $C_0$  and  $C$  are the capacitance per unit area of a grain boundary biased, respectively, with zero and  $V$  volts.

The density of states  $N_{IS}$  at the interface between the grain and the intergranular layer was estimated using

$$N_{IS} = \left(\frac{2N_d k \epsilon_0 \phi}{q}\right)^{1/2}. \quad (2)$$

Thus, the interpretation of Alim et al. [20] to characterize the  $C$  vs.  $V$  characteristics of the dense ZnO-based varistor ceramics and the approach of Mukae et al. [19], were used to elucidate the presence of a Schottky-like barrier and to characterize the nature of the barrier formed in highly dense (Sn,Ti)O<sub>2</sub>-based non-ohmic ceramics.

The main goal of this work is to verify the effect of the TiO<sub>2</sub> concentration in microstructural and electrical properties of (Sn<sub>1-x</sub>Ti<sub>x</sub>)O<sub>2</sub> ceramics ( $x = 0.0, 0.5, \text{ and } 1.0$ ) doped with 1.0 mol% CoO and 0.05 mol% Nb<sub>2</sub>O<sub>5</sub> in order to obtain low voltage varistors. The samples were fully electrically characterized, and the results are discussed in detail.

**2 Experimental** The compositions were prepared by mechanical mixing, and milled in isopropyl alcohol media. The reagents used (all analytical grade) were SnO<sub>2</sub> (Cesbra), TiO<sub>2</sub> (Riedel), CoO (Aldrich), and Nb<sub>2</sub>O<sub>5</sub> (Puratronic). The amount of each oxide was calculated in molar percentages, and the composition and nomenclature of the systems used hereinafter are shown in Table 1. The addition of 1.0 mol% of CoO in SnO<sub>2</sub> increases the oxygen vacancies formation

**Table 1** Composition and nomenclature used for the studied systems.

system composition	nomenclature
98.95%Sn + 1.0%Co + 0.05%Nb	SCN
98.45%Sn + 0.5%Ti + 1.0%Co + 0.05%Nb	STCN1
97.95%Sn + 1.0%Ti + 1.0%Co + 0.05%Nb	STCN2

favoring the diffusion process and promotes the densification of the sample. The addition of 0.05 mol% of Nb<sub>2</sub>O<sub>5</sub> increases the electric conductivity of the SnO<sub>2</sub> matrix. The concentrations of TiO<sub>2</sub> were set as 0.5 and 1.0 mol% in order to avoid the miscibility gap according to the phase diagram of the SnO<sub>2</sub>-TiO<sub>2</sub> system [21].

After drying, the powder was calcined at 900 °C for 2 h and then pressed into 12.0 mm × 1.5 mm discs by uniaxial pressing (20 MPa) followed by isostatic pressing at 210 MPa. The discs were sintered in a tubular furnace at 1350 °C for 4 h with a water vapor flux of 50 sccm connected to the tube entrance using heating rate of 5 °C/min and slowly cooled down to room temperature. For each system, five *identical* samples were prepared, and the values presented here are the average values for samples.

The powders were structurally characterized using the X-ray diffraction (XRD) technique. The XRD for the calcinated powders were collected using a Rigaku RINT2000 diffractometer (42 kV and 120 mA) with Cu K $\alpha$  radiation and a  $2\theta$  range between 20 and 80°.

The microstructural characterization of the samples was performed by scanning electron microscopy (SEM) in a Topcom SM-300 microscope. The average grain size was determined using the linear intercept method. The relative densities of the samples were determined by the Archimedes method.

For electrical measurements, the discs were polished, and silver plate was applied on the parallel surfaces to ensure a good electrical contact. A high voltage source measuring unit (Keithley, model 237) was used to acquire room temperature  $J$  vs.  $E$  plots. The nonlinear coefficient ( $\alpha$ ) was obtained from room temperature  $J$  vs.  $E$  curves in the range from  $J = 1.0$  to 10.0 mA/cm<sup>2</sup>. The breakdown electric field ( $E_b$ ) was taken as the electric field when the current density through the sample was 1.0 mA/cm<sup>2</sup>. The sample leakage current ( $I_l$ ) was taken as the current value at 70% of the breakdown electric field ( $E_b$ ). The samples were also submitted to dc electrical measurements at different temperatures; i.e., the pellets were placed in a sample holder inside a furnace and measurements were made at temperatures ranging from 25 to 200 °C.

Impedance measurements were obtained by using a frequency response analyzer (HP 4192 A) at frequencies ranging from 5 Hz to 13 MHz using voltage amplitude of 1 V and with a dc bias voltage from 0 to 35 V.

**3 Results and discussion** The crystalline structure of the STCN1 and STCN2 powder systems was analyzed by XRD and the results are illustrated in Fig. 1. All peaks in the diffractogram can be indexed as the cassiterite SnO<sub>2</sub> phase, and the relative intensities do not present any preferential orientation. Figure 1 does not show any secondary phases inside the limit of detection of the XRD technique which is below 1 mol%.

Figure 2 illustrates SEM micrographs of the samples sintered at 1350 °C for 4 h. The images reveal that the systems are very dense and are composed of homogeneous

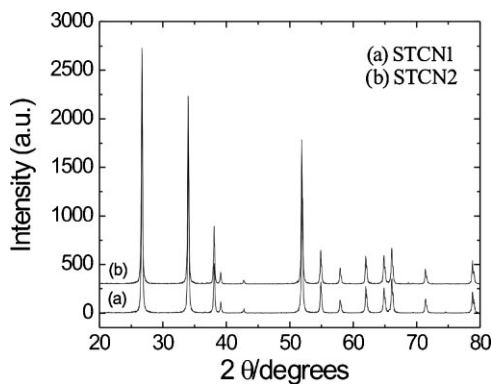


**Figure 1** XRD pattern of the powder heat treated at 900 °C for 2 h: (a) STCN1 and (b) STCN2.

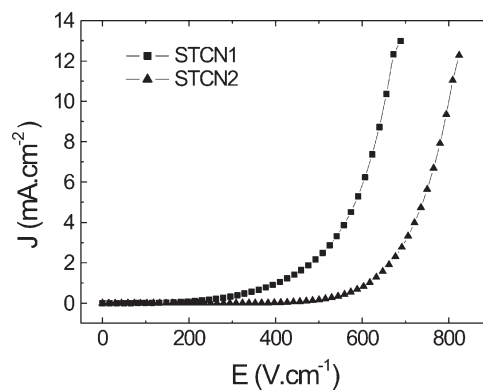


**Figure 3**  $I$ - $V$  plots of systems sintered at 1350 °C/4 h.

grains. Density and mean grain size values are illustrated in Table 2, and the high value of relative density is in agreement with SEM observations. Both the density and the mean grain size of systems with  $\text{TiO}_2$  are significantly larger than the ones for the system without this dopant. The addition of  $\text{TiO}_2$ , which generates oxygen vacancies during sintering in the SCN system, caused an increase in the relative density and in the grain size. This effect should be enhanced by the water vapor atmosphere during sintering. The interaction of the water molecules with the surface of the particles increases both the diffusion process and the densification rate and, consequently the grain size growth [22]. In addition, SEM results demonstrate that there are no observed precipitates at triple points of the grain boundary (which is common for Mn-doped tin dioxide [6, 23]), and only Co-rich segregates should exist at grain boundaries. These segregates cannot be observed by SEM [22], but they are mainly responsible for effective potential barrier formation.

Figure 3 shows the  $J$  vs.  $E$  plot for STCN1 and STCN2 systems. Both systems present a high nonlinear behavior, but the STCN1 system has a greater conductivity in the region below the breakdown electric field ( $E_b$ ) which can jeopardize the nonlinear coefficient. In fact, as shown in Table 2, the nonlinear coefficient for the STCN2 system is almost twice the value for the STCN1 system and is also slightly larger than the value found for the system without  $\text{TiO}_2$  as a dopant. Conversely, Table 2 shows that  $E_b$  decreases significantly with the addition of  $\text{TiO}_2$  with values of about 100 V/cm (in

agreement with the literature results) indicating that these compositions may be applied in low voltage transient suppressor devices [24]. The superscripts in the  $\alpha$  and  $E_b$  values are the standard deviation of measurements. The large grain size presented in STCN systems explains the decrease in the breakdown electric field observed in Table 2 because the number of effective potential barriers per unit of length decreases when the average grain size increases. Leakage current values presented in Table 2 show that increasing the  $\alpha$  value decreases the leakage current explained due to the number of effective barriers in the system. If most potential barriers are effective, the electrons cannot cross the grain boundary region, and no leakage is observed. Also, the value of the nonlinear coefficient is dependent on the number of effective barriers, and Table 2 shows that the system with a minor leakage current value possesses the greater  $\alpha$  value, as expected.

Figure 4 shows the  $\ln J$  vs.  $E^{0.5}$  curves for the systems studied at different temperatures. For a low applied electrical field, there is a strong influence of temperature on the electrical conductivity; i.e., the electrical conductivity increases when the temperature increases, which is a typical behavior of semiconductors. However, for high values of an applied electric field, the electrical conductivity is almost independent of the temperature, and the action of the electric field can distort the potential barrier at the interface, promoting a decrease of the height of the potential barrier and facilitating the electronic transport (a typical Schottky process of conduction). The response observed in Fig. 4 indicates that a Schottky barrier is present in the grain boundary region which is in agreement with the findings for

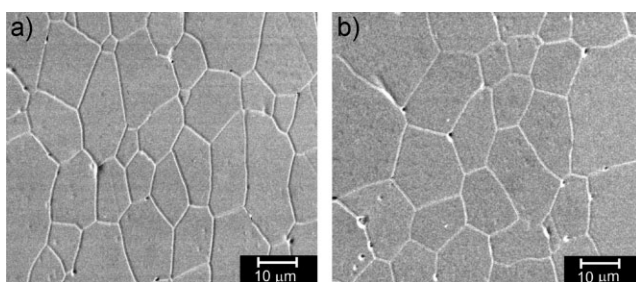


**Figure 2** Micrographies of the systems sintered at 1350 °C: (a) STCN1 and (b) STCN2.

**Table 2** Nonlinear coefficient ( $\alpha$ ), breakdown electrical field ( $E_b$ ), leakage current ( $I_l$ ), relative density ( $d_R$ ), and average grain size ( $L$ ) of the samples sintered at 1350 °C/4 h.

sample	$\alpha$	$E_b$ (V/cm)	$I_l$ (A)	$d_R$ (%)	$L$ ( $\mu\text{m}$ )
SCN [9]	8.0	1870	$8.03 \times 10^{-5}$	96.3	9.0
STCN1	$4.9^{0.2}$	$410^9$	$26.6 \times 10^{-5}$	99.7	35
STCN2	$8.7^{0.3}$	$617^{12}$	$3.86 \times 10^{-5}$	99.7	38

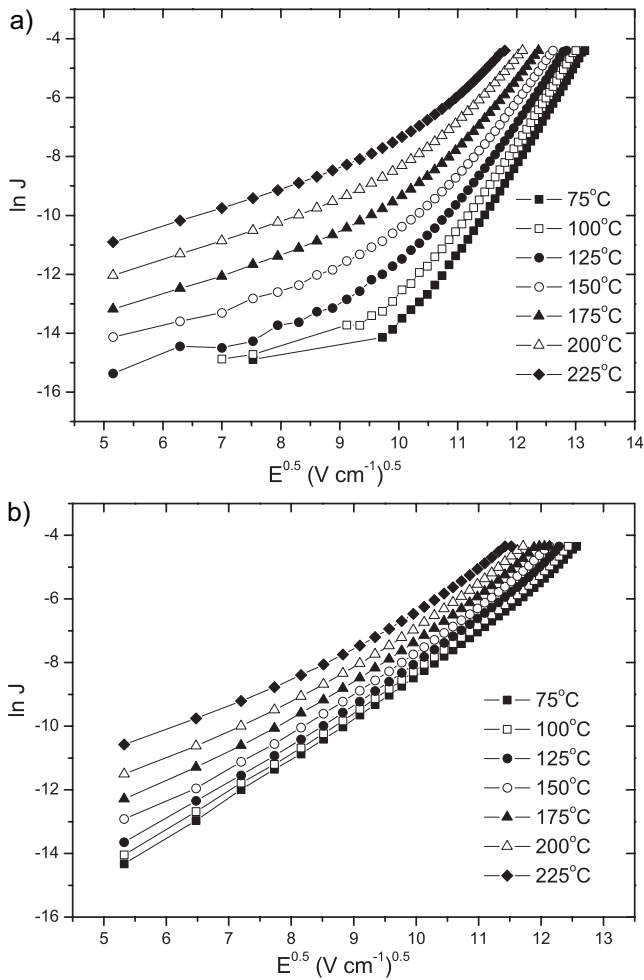


**Figure 4** Characteristic plots of  $\ln J$  vs.  $E^{0.5}$  at different temperatures for the systems: (a) STCN1 and (b) STCN2.

SnO<sub>2</sub>-based varistors. Figure 4 data shows that the potential barrier height of systems studied was determined according to Schottky approaches [7, 25], and the results are shown in Table 3, which also presents values of potential barrier characterization following the Mukae equation [19]. The values obtained for the STCN systems are very close to the value obtained for the system without TiO<sub>2</sub>, but STCN2 presents the highest barrier height. The potential barrier is mainly responsible for the varistor response of ceramics, and the STCN2 system should present the highest  $\alpha$  value which is in agreement with the results presented in this work.

**Table 3** Barrier height ( $\phi$ ),  $\omega$ ,  $N_d$ , and  $N_{IS}$  values for Schottky-type potential barrier of sintered system at 1350 °C/4 h.

sample	$\phi^a$ (eV)	$\phi^b$ (eV)	$\omega$ ( $\times 10^{-8}$ m)	$N_d$ ( $\times 10^{22}$ m <sup>-3</sup> )	$N_{IS}$ ( $\times 10^{15}$ m <sup>-2</sup> )
SCN	0.49 [7]	1.01 [26]		48.2 [26]	27.5 [26]
STCN1	0.44	0.58	1.2	1.51	3.60
STCN2	0.56	0.71	1.4	1.97	3.90

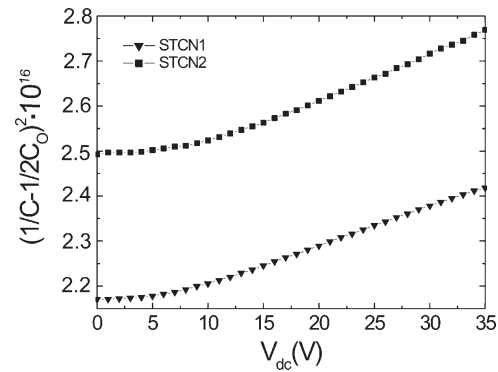


**Figure 5** Mott-Schottky behavior for the systems STCN1 and STCN2 sintered to 1350 °C/4 h.

The Mott-Schottky plot from impedance data using the Alim approach and Mukae equation is shown in Fig. 5 for STCN1 and STCN2 systems. A good linear relationship can be seen between the capacitance reciprocal by the dc bias plot, confirming that the barriers formed at grain boundaries are back-to-back Schottky-type [26]. The capacitance frequency dependence used in conjunction with the information of grain size reflects the averaged Mott-Schottky response of any junction within the SnO<sub>2</sub> varistor device [26]. Table 3 presents  $\phi$ ,  $\omega$ ,  $N_d$ , and  $N_{IS}$  values from this averaged Mott-Schottky response. The values obtained from different methods differ slightly, but both values indicate that the STCN2 system has a higher potential barrier than the STCN1 system which agrees with  $\alpha$  values obtained. The potential barrier width and the number of donor and interfacial states are very close to the values obtained for the SCN system. Therefore, we can infer that the addition of TiO<sub>2</sub> does not significantly alter the potential barrier itself, and the main modification of this dopant is the increased average grain size. This effect reduces the number of potential barriers per unit of length in the sample and, consequently reduces the breakdown electrical field. Notably, results indicate that percentage of the number of effective potential barriers in SCTN2 is not significantly altered in comparison to the SCN system which can be seen by the  $\alpha$  and height barrier values of both systems. However, the total number of barriers is minor in the SCTN2 system, resulting in a lower breakdown electric field value.

The results show that it is possible to achieve a low voltage SnO<sub>2</sub>-based varistor by adding TiO<sub>2</sub> as a dopant. The addition of (+3) and (+5) transition metal oxides (e.g., CoO and Nb<sub>2</sub>O<sub>5</sub>, respectively) is also feasible to obtain good varistor's parameters.

**4 Conclusion** The influence of the addition of the TiO<sub>2</sub> on the microstructure and electrical behavior of doped SnO<sub>2</sub> was investigated. The TiO<sub>2</sub> addition in 0.5 and 1.0 mol% yield  $E_b$  equal to 410 and 617 V/cm, respectively, promoting these compositions as candidates for low voltage varistors. The main influence observed by the addition of TiO<sub>2</sub> was a significant increase in the average grain size

compared to the SnO<sub>2</sub>-based varistor which induced a substantial decrease in the breakdown electric field. The electrical characterization indicated that the potential barrier at the grain boundary region is a back-to-back Schottky-type, and the number of effective barriers is not significantly altered by the addition of TiO<sub>2</sub>.

**Acknowledgements** We would like to thank the Brazilian research funding agencies CNPq, FAPESP, and CAPES for the financial support of this research project.

## References

- [1] G. S. V. Coles, G. Williams, and B. Smith, *Sens. Actuators B* **1**, 7 (1991).
- [2] Z. M. Jarzebski and J. P. Marton, *J. Electrochem. Soc.* **123**, 229C (1976).
- [3] Z. M. Jarzebski and J. P. Marton, *J. Electrochem. Soc.* **123**, 199C (1976).
- [4] J. A. Cerri, E. R. Leite, D. Gouvea, E. Longo, and J. A. Varela, *J. Am. Ceram. Soc.* **79**, 799 (1996).
- [5] D. Gouvea, A. Smith, and J. P. Bonnt, *Eur. J. Solid Inorg. Chem.* **33**, 1015 (1996).
- [6] P. R. Bueno, M. O. Orlandi, L. P. G. Simoes, E. R. Leite, E. Longo, and J. A. Cerri, *J. Appl. Phys.* **96**, 2693 (2004).
- [7] S. A. Pianaro, P. R. Bueno, P. Olivi, E. Longo, and J. A. Varela, *J. Mater. Sci.: Mater. Electron.* **9**, 159 (1998).
- [8] S. A. Pianaro, P. R. Bueno, E. Longo, and J. A. Varela, *J. Mater. Sci. Lett.* **14**, 692 (1995).
- [9] P. A. Cox, R. G. Egdell, C. Harding, W. R. Patterson, and P. J. Tavener, *Surf. Sci.* **123**, 179 (1982).
- [10] A. C. Antunes, S. R. M. Antunes, S. A. Pianaro, M. R. Rocha, E. Longo, and J. A. Varela, *J. Mater. Sci. Lett.* **17**, 577 (1998).
- [11] M. F. Yan and W. Rhodes, *Appl. Phys. Lett.* **40**, 536 (1982).
- [12] P. Sermon and T. J. Walton, *Solid State Ionics* **101**, 673 (1997).
- [13] M. Q. Li and Y. F. Chen, *Sens. Actuators B* **32**, 83 (1996).
- [14] F. Stuki and F. Greuter, *Appl. Phys. Lett.* **57**, 446 (1990).
- [15] P. R. Bueno, E. Camargo, E. Longo, E. R. Leite, S. A. Pianaro, and J. A. Varela, *J. Mater. Sci. Lett.* **15**, 2048 (1996).
- [16] V. C. Sousa, E. R. Leite, J. A. Varela, and E. Longo, *J. Eur. Ceram. Soc.* **22**, 1277 (2002).
- [17] M. Radecka, P. Pasierb, K. Zakrzewska, and M. Rekas, *Solid State Ionics* **119**, 43 (1999).
- [18] P. R. Bueno, M. R. Cassia-Santos, L. G. P. Simões, J. W. Gomes, E. Longo, and J. A. Varela, *J. Am. Soc.* **85**, 282 (2002).
- [19] K. Mukae, K. Tsuda, and I. Nagasawa, *J. Appl. Phys.* **50**, 282 (1979).
- [20] M. Alim, M. A. Seitz, and R. Hirtle, *J. Appl. Phys.* **63**, 282 (1988).
- [21] S. Nambu and M. Oiji, *J. Am. Ceram. Soc.* **74**, 1910 (1991).
- [22] J. A. Varela, O. J. Whittemore, and E. Longo, *Ceram. Int.* **16**, 282 (1990).
- [23] M. O. Orlandi, P. R. Bueno, and E. Longo, *Phys. Status Solidi A* **205**, 383 (2008).
- [24] P. R. Bueno, J. A. Varela, and E. Longo, *J. Eur. Ceram. Soc.* **28**, 505 (2008).
- [25] H. R. Philipp and L. M. Levinson, *J. Appl. Phys.* **46**, 3206 (1975).
- [26] P. R. Bueno, M. R. Cassia-Santos, E. R. Leite, E. Longo, J. Bisquert, G. Garcia-Belmonte, and F. Fabregat-Santiago, *J. Appl. Phys.* **88**, 6545 (2000).